NASA TN D-457

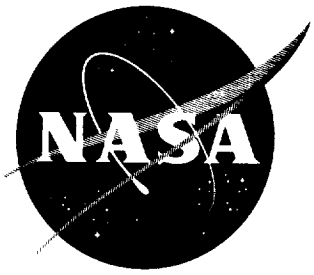

TECHNICAL NOTE

D-457

STRUCTURAL CONSIDERATIONS OF INFLATABLE REENTRY VEHICLES

By Robert W. Leonard, George W. Brooks,
and Harvey G. McComb, Jr.

Langley Research Center
Langley Field, Va.

NATIONAL AERONAUTICS AND SPACE ADMINISTRATION

WASHINGTON

September 1960

NATIONAL AERONAUTICS AND SPACE ADMINISTRATION

TECHNICAL NOTE D-457

STRUCTURAL CONSIDERATIONS OF INFLATABLE REENTRY VEHICLES

By Robert W. Leonard, George W. Brooks,
and Harvey G. McComb, Jr.

SUMMARY

The state of the design art for inflated structures applicable to reentry vehicles is discussed. Included are material properties, calculations of buckling and collapse loads, and calculations of deflections and vibration frequencies. A new theory for the analysis of inflated plates is presented and compared with experiment.

INTRODUCTION

One vehicle which has been proposed as a possible device for achieving manned reentry from orbital flight is the inflatable reentry glider. In this paper some of the problems and properties which must be considered in the design of vehicles of this type are discussed.

It is important to note the state of material availability for application to inflatable reentry vehicles. The expected maximum temperatures on inflated portions of typical proposed vehicles range as high as 1,500° F. This relatively severe temperature environment indicates that an inflatable reentry glider probably must be constructed of woven fabric of high-temperature-resistant metal wire. This fabric must, in turn, be sealed against loss of air pressure by a suitable temperature-resistant coating. At the present time such materials are not available as "off-the-shelf" items. Additional work is needed to improve the quality of woven fabric, to perfect satisfactory joining techniques, and, especially, to improve the properties of available high-temperature-resistant coatings. In spite of these deficiencies, material development for inflatable reentry vehicles is well advanced and this state has been achieved through a modest effort. Thus, with continued or accelerated effort, materials suitable for the construction of an inflatable reentry glider can probably be available in the near future.

SYMBOLS

A	cross-sectional area of inflated structure
c	distance from beam neutral axis to outer fiber
d	distance from cross-sectional center of pressure to outer fiber
F	force
g	structural damping coefficient
h	depth of airmat plate
I	beam cross-sectional moment of inertia
l	length of beam
M	moment
p	internal pressure
q	lateral load intensity
w	lateral deflection of airmat plate
α,β	angles of rotation of airmat drop cords
σ	normal stress
τ	shear stress

PROPERTIES OF INFLATABLE STRUCTURES

Consider now some of the questions of structural configuration and properties which would enter into the design of inflated reentry vehicles. In figure 1 is shown a typical example of such a vehicle. Note that two basic types of structural elements are represented: the inflated circular cylinder which typifies the fuselage construction and the inflated plate which is used for the wings, fins, and control surfaces. Two possible ways of constructing such pneumatic plates are shown in figure 1. At the lower center is shown a plate consisting of an array of tubes, a sort of inflatable equivalent to multiweb construction.

At the right is shown a different arrangement, called "airmat," which was developed by the Goodyear Aircraft Corporation. Airmat consists of two woven covers which are held a fixed distance apart by a regular array of fibers called "drop cords." This arrangement permits an inflatable wing to be tapered in any desired manner. Furthermore, from the standpoint of its strength in bending, airmat is more efficient than the tubular configuration or any similar configuration of the same depth.

Buckling and Collapse Analysis of Inflated Structures

The higher efficiency of airmat plates has been established by simple buckling and collapse analyses. Such analyses are in common use (for example, see ref. 1) and can apparently be applied to any type of inflated structure. The nature and the accuracy of these analyses are illustrated in figure 2 for the case of a load F applied at the tip of an inflated cylindrical cantilever beam of length l. The ordinate of the plot is bending moment at the root, the applied load times the length; the abscissa is the internal pressure in the cylinder. Two calculated curves are shown. The lower curve gives the root bending moment where local buckles, or wrinkles, first appear at the upper extreme fiber. As indicated at the right in figure 2, this is calculated simply as the moment for which the elementary compressive bending stress Mc/I just cancels the tension stress due to pressure. Since this region of zero stress is very localized, the cylinder can carry still more load before collapsing. As the load is increased, the wrinkle progresses around the cross section. Collapse occurs when the wrinkle has progressed all the way to the lower extreme fibers. At this instant, the root cross section takes on the characteristics of a plastic hinge and approximations to the collapse load can be obtained by an application of the theorems of plastic limit analysis. A simple equivalent way of arriving at an approximate collapse load is as follows. Assume that, at collapse, only the extreme lower fibers carry tension to balance the pressure inside the cylinder as indicated at the lower right in figure 2; then, the resisting "plastic hinge" moment is the resultant pressure force pA times the distance d from these extreme fibers to the line of action of the resultant pressure force. Since the cylinder is in equilibrium, this must also be the moment of the applied load at the instant of collapse. The upper curve on the plot in figure 2 has been calculated in this way.

The accuracy of these simple calculations is shown by the experimental points. These data were obtained from cylinders of two different materials, cotton cloth coated with neoprene and fiber-glass cloth coated with latex. Since the cantilever beam is a statically determinant configuration, the buckling and collapse moments do not depend on material properties. Note that the collapse load for a circular cylinder is about twice the buckling load.

Consider now the application of the simple collapse analysis to the 60° inflated delta wing shown in figure 3. This wing is an example of the tubular construction shown in figure 1, with the webs parallel to the root. Again, a concentrated load is applied at the tip. As a result of the tubular construction, collapse occurs simultaneously along each of the webs and at the root according to both experiment and simple theory. The simple criterion for collapse is applied exactly as before, and the resulting moment at the root is plotted in figure 3 against internal pressure. No buckling curve is shown because this configuration is such that there is no discernible difference between buckling and collapse. The experimental points were obtained from a small model made of cotton cloth coated with neoprene. The agreement of these points with the simple collapse theory is seen to be quite good.

The application of the theorems of plastic limit analysis to the collapse of inflated structures leads to the conclusion that this simple theory gives an upper bound on the collapse load. The results shown in figures 2 and 3 indicate that, in many practical cases, this upper bound is quite close to the true collapse load. Thus, the simple collapse criterion appears to be a very useful tool for rough design calculations. It may be applied to any inflated structure, including airmat wing structures.

Deflection Analysis of Inflated Wings

The foregoing results indicate that the determination of collapse loads may be a relatively easy task for the designer of an inflated reentry vehicle. However, the determination of the deformations of the vehicle or the performance of an aeroelastic analysis is quite another matter. Simple beam theories are not adequate for these tasks and material properties must be taken into account; hence, more comprehensive structural theories are needed. Such a theory has been developed for application to plates of the airmat type.

The new airmat-plate theory is a linear "small-deflection" theory based on the following assumptions. It is assumed that the woven material is elastic but orthotropic, that the pressure inside the airmat does not vary with deformation, and that the drop cords are inextensional but they need not remain perpendicular to the covers. (See fig. 4.) This means that transverse shear deformation of the airmat plate is permitted. The theory can be expressed in terms of the deflection w (see fig. 4) and two drop-cord angles α and β. The angle α is shown in figure 4 and β is a similar angle in a plane normal to the figure.

Actually, the airmat-plate theory turns out to be nothing more than a special form of the well-known theory for plates with transverse

shear flexibility. In this case, transverse shear stiffness is the product of the internal pressure p and the depth h of the airmat. In many practical cases this transverse shear stiffness can be expected to be very low so that much of the deflection of the plate is shear deflection not involving deformation of the material in the covers. The theory has been written for the case of constant depth of the airmat plate and inertia forces have been included. These equations are presented in the appendix. Such factors as aerodynamic forces, nonuniform temperature distributions, and depth variations can be inserted if desired.

Some idea of the usefulness of airmat-plate theory is afforded by the comparison with experiment shown in figure 5. A square airmat plate, made of nylon fabric coated with neoprene, was mounted in such a way as to simulate simple support boundary conditions all around. The plate was 18 inches wide with a depth h of 1.125 inches. A uniform external loading q was applied to the surface of the plate at different values of the internal pressure p. Resulting values of the center deflection w, in terms of the depth h of the plate, are plotted in figure 5 against the load q. Data points are shown for three values of internal pressure: 5, 9, and 14 pounds per square inch in excess of the external pressure.

Effective orthotropic elastic constants for the fabric material of the test specimen were obtained from tests of cylinders made from the same material. These constants were used in the new airmat-plate theory (eqs. (A12) to (A14) in the appendix) to calculate deflections of the plate. The calculated values of center deflection, corresponding to each experimental value of internal pressure, are shown by the lines in figure 5. Consider, for a moment, the upper, solid line which gives calculated deflections corresponding to the lowest internal pressure shown on the plot. The importance of transverse shear deformation is shown at the right. It is seen that, for this pressure, approximately three-quarters of the calculated deflection is due to shear alone. Thus, a simple bending analysis which neglects transverse shear flexibility could not be expected to yield even approximately accurate deflections.

In general, the values of deflection calculated with airmat-plate theory are higher than the experimental values. The largest discrepancy is approximately 17 percent at the lowest internal pressure and is believed to be largely due to a peculiarity of the test specimen. The plate specimen used was restrained from shear deformation near its edges by heavy reinforcement which would not be typical of inflated-wing construction. The theory, on the other hand, assumes the plate to be flexible in shear over its whole width, and, hence, can be expected to yield higher deflections especially at the low pressure where shear flexibility is so important. At the highest pressure (the lowest curve), where shear deformation is somewhat less important, the agreement is seen to be quite good.

Material Properties of Fabrics

It is of interest to note in figure 5 that, at each pressure, the experimental points lie approximately on a straight line. This indicates that the behavior of the experimental plate specimen was indeed very nearly linear. Thus, the fabric material of the specimen appears to exhibit linear stress-strain behavior for the range of stress imposed. In spite of this local linear behavior, the stress-strain curve is, on the whole, typically nonlinear. This point is illustrated by the typical stress-strain curves for fabric which are shown in figures 6 and 7.

A single layer of simply woven fabric such as that shown in figure 6 has two sets of perpendicular fibers which are commonly called the warp and the fill fibers. A sheet of such material is thus orthotropic with axes of symmetry in these two perpendicular directions. In the plot in figure 6 is shown a typical stress-strain curve for such a fabric in a state of biaxial tension with stresses σ_{warp} and σ_{fill} in the warp and fill directions. The warp stress is plotted against warp strain for a constant value of the fill stress. Other values of fill stress correspond to different curves as illustrated by the dashed curve for zero fill stress. The initial, curved portion of the stress-strain curve corresponds to the straightening of the warp fibers and bending of the fill fibers as the warp stress is applied; hence, material behavior in this range depends strongly on the tightness of the weave and on the fill stress maintained in the other direction. After this process of straightening and bending of the fibers is nearly complete, the stress-strain behavior depends more on the properties of the material. This curve was based on a linearly elastic fiber material such as metal or fiber glass. Thus, an inflatable reentry structure made from such material might be expected to deform linearly if pressurization has stressed the fabric to this extent.

Note that, in unloading, the curve deviates significantly from the loading path in the lower nonlinear range. This deviation occurs even for fabrics made of linear material. Possible reasons are friction between fibers and exceeding the elastic limit in the fiber straightening process.

In figure 7 is plotted a typical shear stress-strain curve for a simply woven fabric. It is apparent that, at low strains, shear resistance depends strongly on coating characteristics and on friction between the fibers. The friction, in turn, depends strongly on the tension in the fibers. Even for linear fiber material the shear curve is commonly nonlinear and an effective elastic modulus must be assumed for use in a linear elastic theory. As might be expected, the effective shear modulus of simply woven fabrics is generally low; a typical value is one-tenth of the tension modulus as compared with four-tenths for isotropic engineering metals. However, the shear modulus can be raised to nearly

this level simply by adding a bias ply, a second layer of fabric oriented at 45° to the first. The upswing at very high shear strains in figure 7 is primarily attributed to bearing pressure between the fibers. For shear of fabrics, it is common for the unloading curve to depart widely from the loading curve as shown, apparently as a result of friction losses.

One more interesting property of fabrics might be mentioned. Poisson's ratio for a woven fabric sheet is largely associated with the stresses in one direction bending the fibers in the other. Thus, Poisson's ratio depends strongly on the weave and the biaxial stress ratio and some rather unusual values can be obtained; in fact, values of Poisson's ratio much higher than 1 are theoretically possible.

It should be pointed out that, as a result of the longstanding interest in balloons and nonrigid airships, there is in existence a fairly large body of literature on fabric properties in general. However, data on metal fabrics are lacking.

Dynamic Behavior of Inflatable Structures

In addition to material properties and static structural behavior, the designer of an inflatable reentry glider must concern himself with such facets of dynamic structural behavior as vibration modes and frequencies, noise response, and flutter. In order to determine the type of dynamic behavior to be expected from inflated structures, vibration tests have been conducted at the Langley Research Center on simple inflated models. Some results of these tests are shown in figure 8.

The upper plot in figure 8 shows typical experimental response curves of a 60° inflated delta-wing model at a given internal pressure. The structure is tapered airmat and the material is silk cloth with a latex coating. Measured amplitude is plotted against vibration frequency with both quantities expressed in terms of values at the first natural frequency. The first mode is found to be a bending mode with the node line at the root. The amplitude is measured at the tip as indicated by the letter A on the small sketch. Note that the peak is relatively sharp with a distinct resonant frequency. The corresponding value of the structural damping coefficient ($g = 0.073$) is only two to four times values found for conventional metal structures. The second mode is a torsion mode with the node line as shown on the sketch. In this case the amplitude was measured at a point along the leading edge. Again the resonant frequency is sharply defined and, in fact, the damping coefficient is 0.045, lower than in the first mode.

Response curves, such as those in the upper plot of figure 8, were obtained for both modes at several values of internal pressure. The

plot at the bottom shows the increase of resonant frequency with internal pressure for both the first and second modes. The structural damping coefficients maintained the same order of magnitude at all pressures.

The results in figure 8 are evidence that the dynamic behavior of inflated fabric wing structures is much like the dynamic behavior of conventional metal wing structures. Thus, the many dynamic problems which must be considered in the design of conventional structures may also be problems for the designer of inflated structures. For example, flutter analysis probably should be an important part of the design process for inflatable reentry gliders.

The linear airmat-plate theory presented in the appendix may be readily adapted for vibration and flutter analysis. Its use in the calculation of natural vibration frequencies is illustrated in figure 9.

The structure considered is the same square airmat plate of nylon and neoprene discussed previously. The plot in figure 9 gives the lowest three natural frequencies of this plate as a function of internal pressure. An indication of corresponding mode shapes is shown by the small figures in the key. Thus the lowest frequency corresponds to a single half sine wave in both directions and no node line appears. The next two mode shapes differ only in the direction of the single node line. The slight difference in frequency for these two shapes is primarily due to the directional elastic properties of the fabric cover material. The points are measured values of frequency whereas the curves were calculated by the use of airmat-plate theory. The agreement is seen to be reasonably good.

CONCLUDING REMARKS

The state of structural design capability for the inflatable reentry glider can be summarized by the following remarks. In the first place, it must be pointed out that material development for application to inflatable reentry vehicles is not yet complete. In particular, more work is needed on joining techniques and on fabric coatings which will withstand temperatures up to and, perhaps, somewhat beyond 1,500° F. From the standpoint of the structural design process, however, the designer has at his disposal simple, but adequate, procedures for the calculation of buckling and collapse loads on inflatable structures. He also has available a linear theory for the deflection analysis of inflatable wing structures. This linear theory can yield reasonably accurate results in spite of nonlinearities which characterize the mechanical properties of fabric materials. It can also be adapted for

vibration and flutter analysis which apparently should be an important part of the design process. Thus, one might conclude that, while there is much work yet to be done, the creation of rational design procedures for inflated reentry vehicles is indeed possible.

Langley Research Center,
National Aeronautics and Space Administration,
Langley Field, Va., April 12, 1960.

APPENDIX

A LINEAR THEORY FOR "AIRMAT" PLATE

INTRODUCTION

This appendix contains a very brief outline of the derivation of the linear differential equations and boundary conditions for a rectangular plate of constant-depth "airmat" construction. The basic assumptions underlying the theory are mentioned in the paper and listed in figure 4. The presence of a bulkhead at the edges of the plate is not explicitly accounted for in the theory. It is assumed, however, that some mechanism exists along the edges of the plate to keep the internal air from escaping.

SYMBOLS

a,b	dimensions of plate in x- and y-directions, respectively
E_W,E_F	Young's modulus in warp direction and fill direction of the covers, respectively
G	modulus of rigidity for cover material
h	depth of plate
M_x,M_y,M_{xy}	plate moments and twist associated with differences between stress resultants in top and bottom covers
m	mass of the plate per unit middle plane area
N_x,N_y,N_{xy}	plate stress resultants associated with sums of stress resultants in top and bottom covers
p	internal pressure
q	external distributed lateral load
t	thickness of each cover
u,v,w	plate displacements, the average of the displacements in the top and bottom covers in x-, y-, and z-directions, respectively

V	volume of plate
W	external work
x,y,z	coordinates
α,β	angles between drop cords and Z-axis in X,Z and Y,Z planes, respectively, associated with differences between displacements in top and bottom covers
μ_{WF},μ_{FW}	Poisson's ratios
Π_C	strain energy in covers
Π_I	work done against internal pressure

Comma preceding a subscript denotes differentiation with respect to the subscript. Dots over a symbol denote differentiation with respect to time.

ANALYSIS

The coordinate system is chosen so that the middle plane of the plate lies in the X,Y plane as shown in the following sketch:

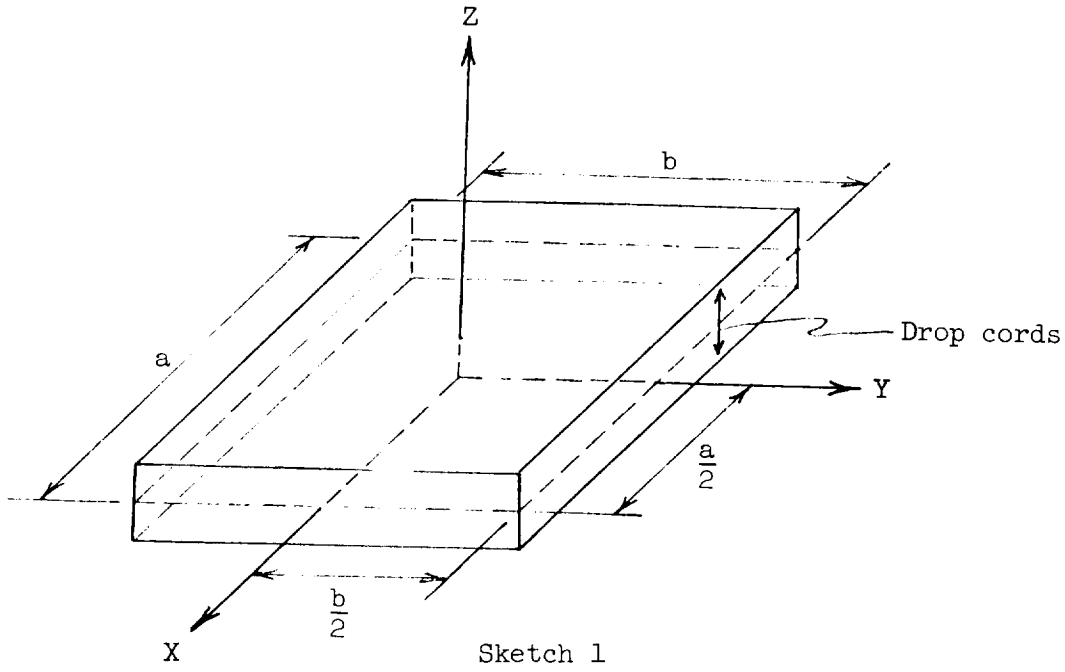

Sketch 1

An element is removed from the plate and shown in the following sketch:

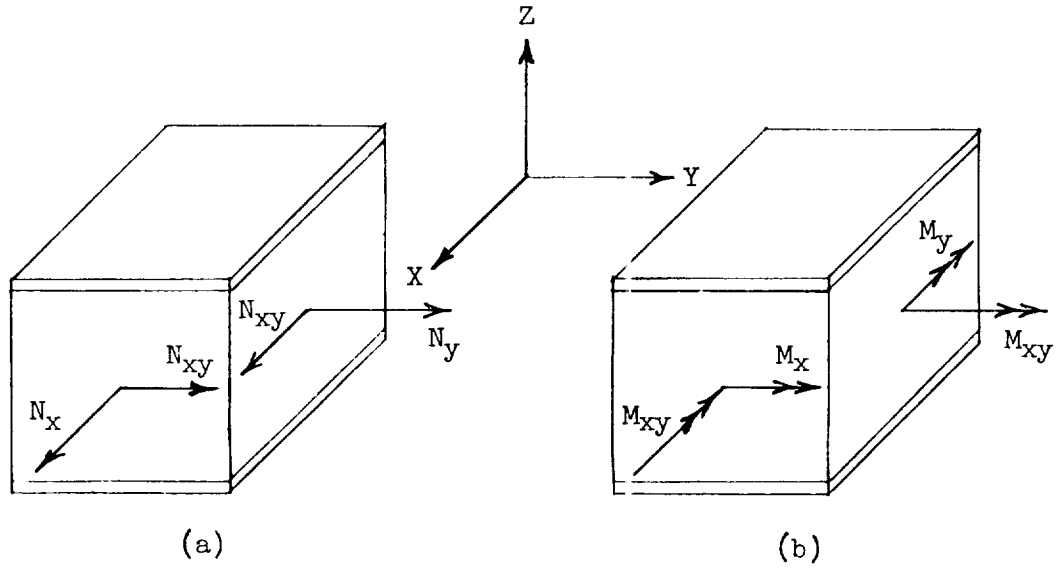

Sketch 2

The plate stress resultants are shown acting on the element in the positive senses in sketch 2(a). In sketch 2(b) the plate moments and twist are shown in the positive senses.

The theory is developed through an application of the principle of minimum potential energy which requires

$$\delta\left(\Pi_C + \Pi_I - W\right) = 0$$

In this expression Π_C represents the strain energy in the covers, Π_I represents the work done against the internal pressure due to change in volume of the plate, and W represents the potential energy of the external loads. Since a linear theory is sought, in writing expressions for Π_C, Π_I, and W, it is permissible to neglect all terms of order higher than 2 in products of the plate displacements, drop-cord angles, or their derivatives.

The variation of the strain energy in the covers can be written in terms of the plate stress resultants and the plate displacements and drop-cord-angles as follows:

$$\delta\Pi_c = \int_{-b/2}^{b/2} \int_{-a/2}^{a/2} \left[N_x \delta\left(u_{,x} + \frac{1}{2} w_{,x}^2\right) + N_y \delta\left(v_{,y} + \frac{1}{2} w_{,y}^2\right) + N_{xy} \delta\left(u_{,y} + v_{,x} + w_{,x} w_{,y}\right) + M_x \delta\alpha_{,x} + M_y \delta\beta_{,y} + M_{xy}\left(\delta\alpha_{,y} + \delta\beta_{,x}\right) \right] dx\, dy$$

In order to obtain $\delta\Pi_I$, it is necessary to calculate the change in volume of the plate caused by displacements and drop-cord angles u, v, w, α, and β. This change in volume is obtained by calculating the final volume of the plate after an arbitrary displacement and subtracting the initial volume. The volume of the deformed plate is calculated from the surface integral (see, for example, ref. 2)

$$V = -\iint_S z\, dx\, dy$$

where x, y, and z represent the coordinates of points in the deformed plate surfaces and the surface integral must be evaluated over the six outside surfaces of the plate. The quantity $\delta\Pi_I$ is the negative of the product of the internal pressure and the variation of the increase in volume. The result is

$$\delta\Pi_I = -p\delta \int_{-b/2}^{b/2} \int_{-a/2}^{a/2} h \left[u_{,x} + v_{,y} - \alpha w_{,x} - \beta w_{,y} - \frac{\alpha^2}{2} - \frac{\beta^2}{2} + u_{,x} v_{,y} - u_{,y} v_{,x} + \frac{h^2}{4}\left(\alpha_{,x}\beta_{,y} - \alpha_{,y}\beta_{,x}\right) \right] dx\, dy + \int_{-b/2}^{b/2} \frac{h^3}{12}\left(\alpha_{,y}\beta - \alpha\beta_{,y}\right)\Big|_{-a/2}^{a/2} dy + \int_{-a/2}^{a/2} \frac{h^3}{12}\left(\alpha\beta_{,x} - \alpha_{,x}\beta\right)\Big|_{-b/2}^{b/2} dx$$

where the symbol $\Big|_{-a/2}^{a/2}$ means that the integrand at $x = -\frac{a}{2}$ is subtracted from the integrand at $x = \frac{a}{2}$, etc.

The external-work term includes inertia contributions. The expression for the variation of the external work is

$$\delta W = \int_{-b/2}^{b/2} \int_{-a/2}^{a/2} \left(q\delta w - m\ddot{w}\delta w - m\ddot{u}\delta u - m\ddot{v}\delta v - \frac{h^2}{4} m\ddot{\alpha}\delta\alpha - \frac{h^2}{4} m\ddot{\beta}\delta\beta \right) dx\, dy$$

The indicated variational operation is now carried through and certain terms are integrated by parts. There results from this procedure an integral over the area of the middle surface of the plate and integrals along the edges of the plate. Each term in the area integral contains one of the following quantities: δu, δv, δw, $\delta\alpha$, or $\delta\beta$. The coefficients of these five quantities can be set equal to zero independently by the arguments of the calculus of variations. This procedure yields the following partial differential equations of equilibrium for the airmat plate:

$$N_{x,x} + N_{xy,y} = m\ddot{u} \tag{A1}$$

$$N_{y,y} + N_{xy,x} = m\ddot{v} \tag{A2}$$

$$\left(N_x w_{,x}\right)_{,x} + \left(N_y w_{,y}\right)_{,y} + \left(N_{xy} w_{,x}\right)_{,y} + \left(N_{xy} w_{,y}\right)_{,x} + ph\alpha_{,x} + ph\beta_{,y} + q = m\ddot{w} \tag{A3}$$

$$M_{x,x} + M_{xy,y} - ph\left(\alpha + w_{,x}\right) = \frac{h^2}{4} m\ddot{\alpha} \tag{A4}$$

$$M_{y,y} + M_{xy,x} - ph\left(\beta + w_{,y}\right) = \frac{h^2}{4} m\ddot{\beta} \tag{A5}$$

Similar arguments applied to the boundary integrals lead to two sets of boundary conditions. Along $x = \pm \frac{a}{2}$

$$\delta u = 0 \quad \text{or} \quad N_x - ph\left(1 + v_{,y}\right) = 0$$

$$\delta v = 0 \quad \text{or} \quad N_{xy} + phu_{,y} = 0$$

$$\delta w = 0 \quad \text{or} \quad N_x w_{,x} + N_{xy} w_{,y} + ph\alpha = 0$$

$$\delta\alpha = 0 \quad \text{or} \quad M_x - \frac{ph^3}{12}\beta_{,y} = 0$$

$$\delta\beta = 0 \quad \text{or} \quad M_{xy} + \frac{ph^3}{12}\alpha_{,y} = 0$$

Along $y = \pm \frac{b}{2}$ the conditions are the same as those for $x = \pm \frac{a}{2}$ except that u and v, α and β, and x and y are interchanged.

In addition to the differential equations of equilibrium and boundary conditions for the plate, six stress-strain relations are required to specify the problem completely. The form of these stress-strain relations depends on the properties of the cover material. For example, if the covers are a simply woven fabric (fig. 6) with the X- and Y-axes assumed, for simplicity, to lie along the warp and fill directions of the fabric, the linearized stress-strain relations are

$$N_x = 2\left(A_{11}u_{,x} + A_{12}v_{,y}\right)$$

$$N_y = 2\left(A_{21}u_{,x} + A_{22}v_{,y}\right)$$

$$N_{xy} = 2A_{33}\left(u_{,y} + v_{,x}\right)$$

$$M_x = \frac{h^2}{2}\left(A_{11}\alpha_{,x} + A_{12}\beta_{,y}\right)$$

$$M_y = \frac{h^2}{2}\left(A_{21}\alpha_{,x} + A_{22}\beta_{,y}\right)$$

$$M_{xy} = \frac{h^2}{2}A_{33}\left(\alpha_{,y} + \beta_{,x}\right)$$

where

$$A_{11} = \frac{E_W t}{1 - \mu_{WF}\mu_{FW}}$$

$$A_{12} = \frac{\mu_{FW} E_W t}{1 - \mu_{WF}\mu_{FW}}$$

$$A_{21} = \frac{\mu_{WF} E_F t}{1 - \mu_{WF}\mu_{FW}}$$

$$A_{22} = \frac{E_F t}{1 - \mu_{WF}\mu_{FW}}$$

$$A_{33} = Gt$$

When the inertia terms are neglected, the differential equations (eqs. (A1) to (A5)) reduce to

$$N_{x,x} + N_{xy,y} = 0 \tag{A6}$$

$$N_{y,y} + N_{xy,x} = 0 \tag{A7}$$

$$N_x w_{,xx} + N_{x,x} w_{,x} + N_y w_{,yy} + N_{y,y} w_{,y} + N_{xy} w_{,xy} + N_{xy,y} w_{,x} + N_{xy} w_{,yx}$$

$$+ N_{xy,x} w_{,y} + ph\alpha_{,x} + ph\beta_{,y} + q = 0 \tag{A8}$$

$$M_{x,x} + M_{xy,y} - ph(\alpha + w_{,x}) = 0 \tag{A9}$$

$$M_{y,y} + M_{xy,x} - ph(\beta + w_{,y}) = 0 \tag{A10}$$

Use of the equations (A6) and (A7) reduces equation (A8) to

$$N_x w_{,xx} + N_y w_{,yy} + 2N_{xy} w_{,xy} + ph\alpha_{,x} + ph\beta_{,y} + q = 0 \tag{A11}$$

L
1
0
8
0

If the plate stresses result from internal pressure alone so that $N_x = N_y = ph$ and $N_{xy} = 0$, the differential equations (A9), (A10), and (A11) become

$$ph(\alpha + w_{,x})_{,x} + ph(\beta + w_{,y})_{,y} + q = 0 \tag{A12}$$

$$M_{x,x} + M_{xy,y} - ph(\alpha + w_{,x}) = 0 \tag{A13}$$

$$M_{y,y} + M_{xy,x} - ph(\beta + w_{,y}) = 0 \tag{A14}$$

These equations are essentially the governing differential equations for plates with transverse shear flexibility taken into account. (See, for example, ref. 3.) The internal pressure p plays the role of the modulus in the plate transverse shear stiffness.

REFERENCES

1. Topping, A. D.: A Preliminary Study of Methods of Analysis of "Airwall" Structures. GER 5850, Goodyear Aircraft Corp., Feb. 19, 1954.

2. Courant, R.: Differential and Integral Calculus. Vol. II. Interscience Publishers, Inc. (New York), 1952, p. 387.

3. Mindlin, R. D.: Influence of Rotatory Inertia and Shear on Flexural Motions of Isotropic, Elastic Plates. Jour. Appl. Mech., vol. 18, no. 1, Mar. 1951, pp. 31-38.

TYPICAL INFLATABLE REENTRY CONFIGURATION

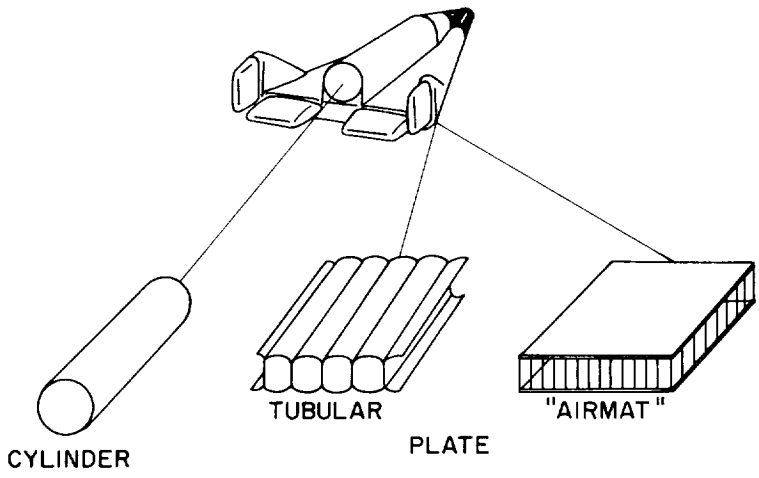

Figure 1

SIMPLE STRENGTH ANALYSIS OF AN INFLATED CYLINDER

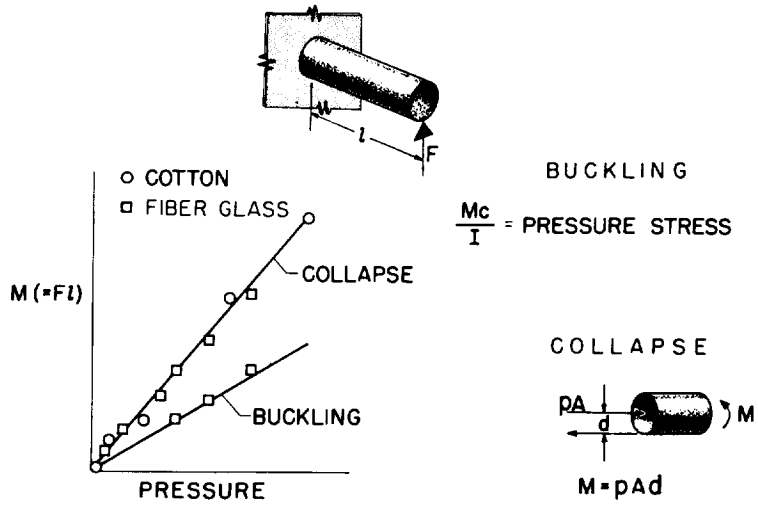

Figure 2

TYPICAL SHEAR PROPERTIES OF FABRICS

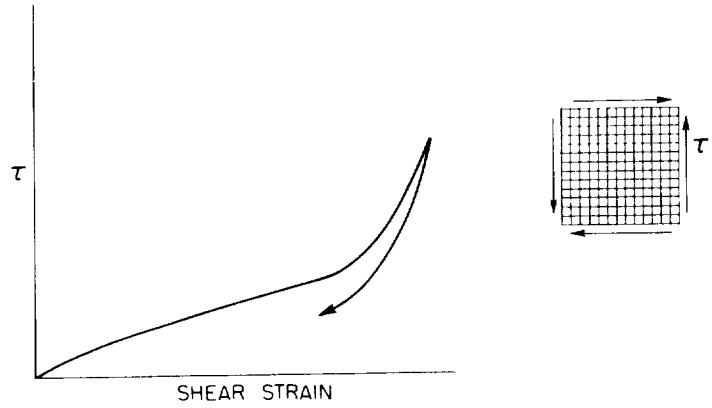

IMPORTANT FACTORS:

COATING CHARACTERISTICS
FRICTION (TENSION)

Figure 7

VIBRATION CHARACTERISTICS OF 60° SILK-LATEX DELTA WING

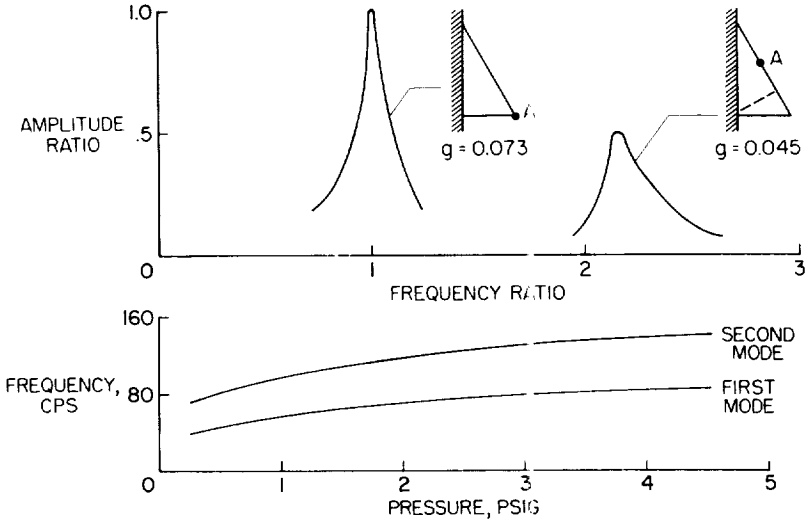

Figure 8

FREQUENCIES OF SQUARE NYLON-NEOPRENE AIRMAT PLATE

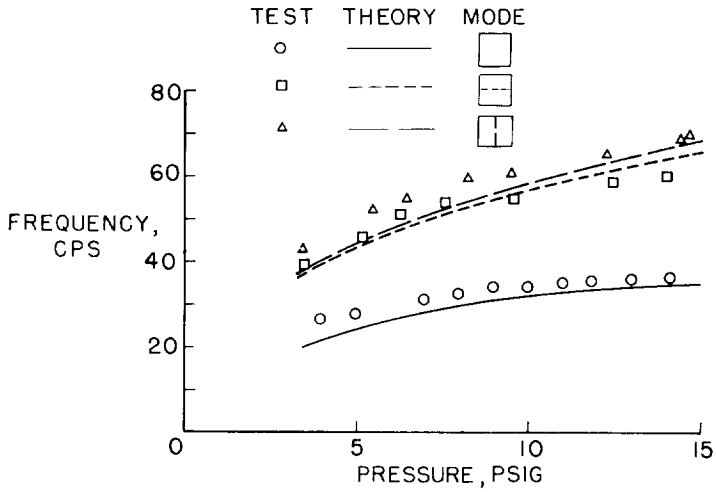

Figure 9